An Energy Management Scheme With Power Limit Capability and an Adaptive Maximum Power Point Tracking for Small Standalone PMSG Wind Energy Systems

Joanne C. Y. Hui, *Member, IEEE*, Alireza Bakhshai, *Senior Member, IEEE*, and Praveen K. Jain, *Fellow, IEEE*

***Abstract*—Due to its high energy generation capability and minimal environmental impact, wind energy is an elegant solution to the growing global energy demand. However, frequent atmospheric changes make it difficult to effectively harness the energy in the wind because maximum power extraction occurs at a different operating point for each wind condition. This paper proposes a parameter-independent intelligent power management controller that consists of a slope-assisted maximum power point tracking (MPPT) algorithm and a power limit search (PLS) algorithm for small standalone wind energy systems with permanent synchronous generators. Unlike the parameter-independent perturb & observe algorithms, the proposed slope-assisted MPPT algorithm preempts logical errors attributed to wind fluctuations by detecting and identifying atmospheric changes. The controller's PLS is able to minimize the production of surplus energy to minimize the heat dissipation requirements of the energy release mechanism by cooperating with the state observer and using the slope parameter to seek the operating points that result in the desired power rather than the maximum power. The functionality of the proposed energy management control scheme for wind energy systems is verified through simulation results and experimental results.**

***Index Terms*—Energy management, maximum power point tracking (MPPT), power electronics, wind energy.**

I. Introduction

WIND power has been experiencing a healthy growth over the years thanks to its ability to produce large amounts of clean power at minimal cost. In Canada, the Canadian Wind Energy Association and the Global Wind Energy Council has forecasted that by 2015, Canada's total installed wind capacity will exceed 10 GW [1]–[3].

To be an effective alternative energy source, wind turbines should extract as much power as possible from the wind when it is available. Each wind turbine has a unique power characteristic due to their aerodynamic profile. The power characteristic dictates that there exists a specific optimal turbine rotational speed for each wind condition that results in maximum power capture. Various types of maximum power point tracking (MPPT) algorithms have been presented in the literature [4]–[20], but they are prone to diverging from the wind system's maximum power curve (MPC) under fluctuating atmospheric conditions and machine aging. In general, the methods can be classified into two main categories: customized algorithms [9], [11] and perturb & observe (P&O)-based algorithms. Customized algorithms typically require external sensors to constantly relay atmospheric information to the controller, whereas P&O algorithms can be further separated into memoryless [5], [10], [12] and adaptive (memory based) [4], [6], [13], [19] algorithms. Due to their parameter independence, memoryless P&O MPPT algorithms not WES specific and can therefore be used for a wide range of WESs. However, since these algorithms are based on the P&O technique, their effectiveness is greatly reduced in the event of frequent wind speed changes. The algorithms proposed in [6] are an example of a sensor-based adaptive algorithm, while those in [13], [14], [17], and [19] are sensorless P&O examples. With regards to the actual MPPT approach, the methods outlined in [4] and [6] use lookup tables to expedite the MPP search procedure for past wind conditions. Xia *et al.* [13], on the other hand, use mathematical relationships to infer MPPs for different wind speed conditions.

In standalone off-grid applications, the goal is not to simply extract the maximum power since there are energy storage limitations. As such, the generated wind energy must be properly regulated. Several works on power management for standalone wind energy systems have been presented [22]–[26]. When there is a surplus of power, it is redirected to an energy "dump" known as a "dummy load" and the excess power is dissipated as heat [22], [26]. Therefore, the challenge of standalone wind systems is to efficiently extract the maximum power from the wind when possible and minimize surplus energy generation to reduce the cost and heat dissipation requirements of the energy dump mechanism.

This paper proposes a parameter-independent intelligent power management controller that consists of a slope-assisted (SA) MPPT and a power limit search (PLS) algorithm for standalone off-grid wind energy systems. The MPPT algorithm uses a derived "slope" relationship-based algorithm that correlates the measured power and speed of the turbine to the system tip speed ratio (TSR). The TSR characterizes the level of aerodynamic efficiency of the turbine; for each wind turbine, maximum power capture occurs at a singular TSR at all wind speeds. The

Manuscript received December 4, 2014; revised March 11, 2015, May 19, 2015, and July 29, 2015; accepted August 31, 2015. Date of publication September 14, 2015; date of current version January 28, 2016. Recommended for publication by Associate Editor Y. Sozer.

The authors are with the Electrical and Computer Engineering Department, Queen's University, Kingston, ON K7L 3N6 Canada (e-mail: 2cyjh@queensu.ca; alireza.bakhshai@queensu.ca; praveen.jain@queensu.ca).

Color versions of one or more of the figures in this paper are available online at http://ieeexplore.ieee.org.

Digital Object Identifier 10.1109/TPEL.2015.2478402

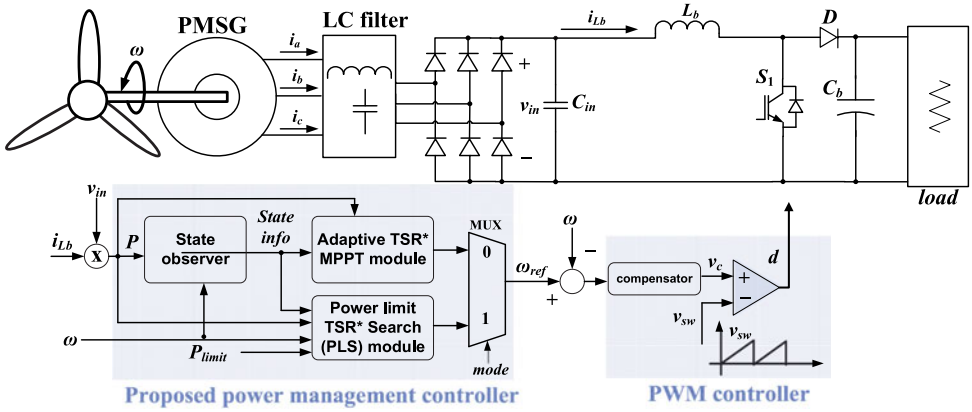

Fig. 1. System diagram with the proposed management control algorithm.

"slope" relationship represents all the power and generator speed values that correspond to a specific TSR. By using this relationship, it allows the algorithm to "remember" the last effective position on the power curve before the atmospheric change and resume its search process following the interruption. The algorithm also stores and analyzes the obtained maximum power points (MPP) to determine an averaged optimal slope–TSR relationship that allows it to accurately infer the location of the MPPs when the wind speed and/or air density conditions change.

The PLS unit, on the other hand, is used to regulate the power generated in high winds to minimize surplus power generation. The PLS algorithm uses a search method that is similar to the adaptive MPPT. However, rather than searching for the MPP, the PLS searches for and maintains the operating points that will result in the desired output power level rather than the MPP. Together, the proposed MPPT and PLS algorithms form a power management controller that regulates the power extraction of the WES in high winds and maintains the highest possible power extraction efficiency at all times. The power management controller autonomously switches between the MPPT and the PLS to regulate the wind turbine energy extraction.

This paper is organized as follows: Section II describes the proposed power management scheme for standalone wind energy systems, in particular, the operating modes between the proposed MPPT controller and the PLS unit are discussed. Section III gives an example and discusses the performance of the proposed work through simulation and experimental results. Section IV provides a conclusion to summarize the features of the proposed work.

II. Description of the Proposed Energy Management Control Scheme

Wind energy is not only suitable for large-scale energy production; small standalone wind systems are ideal for powering remote off-grid areas and individual homes. While grid-connected systems should ideally operate such that the maximum power from the wind is always extracted, standalone off-grid WESs simply cannot always extract the maximum power due to energy storage limitations. The minimization of excess power generation is important in standalone off-grid WESs as it will reduce the size and heat dissipation requirements of the dummy load and, therefore, also reduce the cost of a standalone WES.

The proposed power management controller features a SA MPPT algorithm that is parameter independent, fast, and robust to ambient atmospheric variations and machine parameter shifts due to system aging. The proposed controller also features a PLS algorithm that regulates the WES power generation to minimize the generation of wasted power and burden on the energy dissipation unit. Fig. 1 shows the diagram of the WES with the proposed power management controller. The power stage consists of a three-phase diode rectifier and a boost converter. The proposed power management controller consists of a state observer, a MPPT module, and a PLS module. The state observer is the supervisory unit and it presides over the MPPT and PLS modules to regulate the WES output power. The proposed control scheme does not require any physical sensors that are used to relay the wind speed, temperature, and/or humidity information to minimize cost and sensor error. External sensors like anemometers are often inaccurate due to difficult placement. Rather than relying on external sensors, the controller records and analyzes the electrical behavior of the WES to identify the atmospheric changes that cause the WES to shift from one power curve to another.

The state observer focuses on the abnormalities in the power and generator speed trends to detect atmospheric changes, the system state, and selecting the mode of operation (MPPT or PLS). Given the state information from the state observer, the MPPT and PLS submodules subsequently derive pTSR values to generate the appropriate system references and distinguish between legitimate power changes (due to control adjustments) and compromised power readings (caused by atmospheric changes). When compromised power readings are acknowledged, the active submodule uses the pTSR values to further assess whether the wind speed has increased or decreased.

The observer determines the appropriate module to activate based on the given power limit, atmospheric condition, and the system operating state. By default, the MPPT mode is selected to extract maximum power from the wind and the PLS mode is

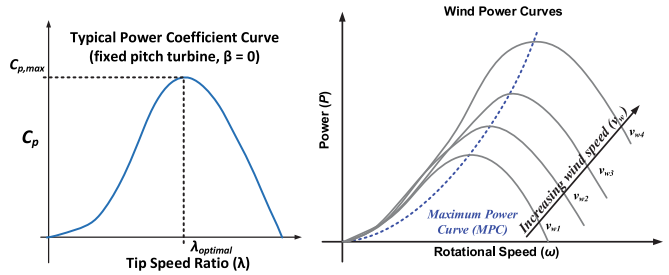

Fig. 2. (a) Power coefficient curves with respect to the pitch angle β. (b) Power curves for a typical fixed-pitch ($\beta = 0$) wind turbine.

only activated when the WES output power exceeds the defined power limit threshold. The controller will only switch from the PLS mode to the MPPT mode when it has identified that the WES output power has dropped below the power limit due to a decrease in wind speed and/or air density. In the following sections, the MPPT and PLS modules will be discussed in detail.

A. SA Methodology

In general, the power captured by the wind turbine is governed by (1), where ρ is the air density, A is the rotor swept area, $C_p(\lambda, \beta)$ is the power coefficient function, λ is the TSR that is given by (2), β is the turbine blade pitch angle, v_w is the wind speed, and ω is the rotational speed

$$P = 0.5\rho A C_p(\lambda, \beta) v_w^3 \tag{1}$$

$$\lambda = \frac{R\omega}{v_w}. \tag{2}$$

Fig. 2(a) illustrates the typical power coefficient curve of a fixed-pitch ($\beta = 0$) wind turbine and it can be seen that there is a singular optimal TSR (denoted by λ_{opt}) that results in maximum power extraction efficiency denoted by $C_{p\max}$. In a fixed-pitch WES, the power extraction efficiency is influenced solely by the C_p function and the TSR (the ratio between the generator rotational speed and the wind speed). While the air density does not affect the power extraction efficiency, it is important to note that it significantly affects the amount of power extracted by the turbine. Therefore, to isolate the effects of wind speed, Fig. 2(b) illustrates the power curves for a fixed-pitch turbine with varying wind speed conditions and the standard air density value at sea level and at 25 °C ($\rho = 1.225$ kg/m^3). The power curves in Fig. 2(b) show that for each v_w, maximum power extraction occurs at a unique operating point (i.e., a unique rotational speed, ω), which is known as the MPP for that wind speed. The MPPs for different wind speeds collectively form a MPC and it can be defined by the relationship: $P \propto k\omega^3$, where k is a constant that describes the turbine aerodynamic characteristics.

The wind turbine's power extraction efficiency (i.e., the system's C_p value) is characterized by the TSR and each TSR value defines all the operating points (i.e., rotational speeds) for all the wind speeds that have the same C_p value. The power management controller revolves around the proposed SA methodology and its premise is to use measureable values (i.e., system output power and rotational speed) to derive a parameter that represents the system's TSR; this parameter is referred to as the slope parameter $m_{\lambda k}$. The slope parameter allows the controller to identify wind speed changes and shortens the MPP search process by allowing the system to revert back to its last TSR state if any anomalies (e.g., wind change or MPP overshoot) occur.

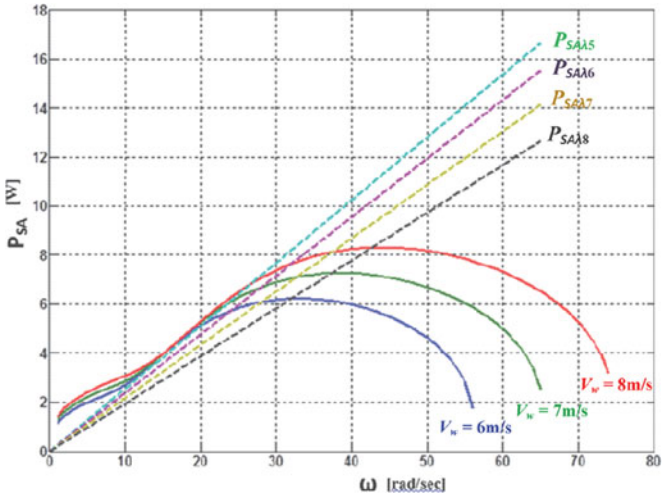

Fig. 3. P_{SA} curves and the corresponding linear $P_{\text{SA},\lambda}(\omega)$ lines that are defined by (4).

Recalling the relationship between the C_p curve and the TSR [see Fig. 2(a)], $C_p(\lambda)$ becomes a constant value ($C_{p,\lambda k}$) for a fixed TSR value (λ_k). By substituting (2) into (1), we obtained

$$P = \frac{1}{2}\rho A C_{p,\lambda k}\left(\frac{R\omega}{\lambda_k}\right)^3. \tag{3}$$

Equation (3) can be further simplified to become (4), where $P_{\text{SA},\lambda k}$ is the linear SA function for a fixed TSR (λ_k) and $m_{\lambda k}$ is the constant slope value of $P_{\text{SA},\lambda k}$ that can be obtained by measuring the output power and the rotational speed [see (5)]

$$P_{\text{SA},\lambda k} = \sqrt[3]{P} = m_{\lambda k}\omega, \quad \text{where}$$
$$m_{\lambda k} = \frac{R}{\lambda_k}\left(\sqrt[3]{\frac{1}{2}\rho A C_{p,\lambda k}}\right) \text{ for a fixed } \lambda_k \tag{4}$$

$$m_{\lambda k} = \frac{\sqrt[3]{P}}{\omega}, \quad \text{for a fixed } \lambda_k. \tag{5}$$

It should be noted that while the TSR is a fixed value, there are multiple ω and v_w combinations that result in the same TSR value (6) since the TSR is defined as a ratio between ω and v_w

$$\lambda_k = \frac{R\omega_1}{v_{w1}} = \frac{R\omega_2}{v_{w2}} = \frac{R\omega_3}{v_{w3}} \cdots = \frac{R\omega_n}{v_{wn}}. \tag{6}$$

The $P_{\text{SA},\lambda k}$ functions for each TSR is plotted with respect to the cubed root of power P_{SA} [expressed as (7)] and the rotational speed in Fig. 2(b). The $P_{\text{SA},\lambda k}$ functions can be represented by its slope $m_{\lambda k}$, given by (5) with its origin located at (0, 0); the slope value $m_{\lambda k}$ (is also referred to as the pseudo-TSR, pTSR, in this paper). Since the slope value is a constant value that represents λ for all wind speeds, from two easily measurable parameters: P and ω. As illustrated in Fig. 3, all the operating

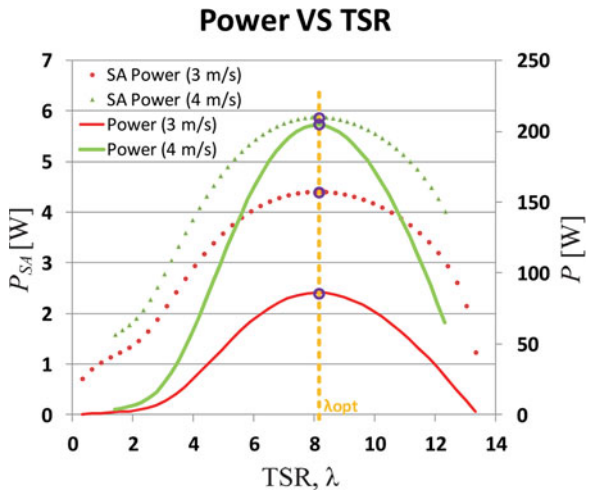

Fig. 4. Both P_{SA} and standard wind power equations show that the MPPs of the system occur at the same optimal TSR value.

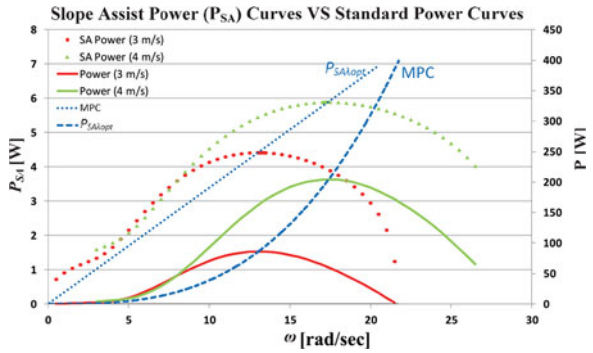

Fig. 5. Comparison of SA power (P_{SA}) curves and standard power curves.

points that correspond to a single pTSR (e.g., all the operating point occurs on the line defined by a single line with the slope $m_{\lambda k}$ correspond to single λ_k and, therefore, a single power coefficient value $C_{p\lambda k}$

$$P_{\mathrm{SA}} = \sqrt[3]{P} = \left(\sqrt[3]{\frac{1}{2}\rho A C_p(\lambda)}\right) v_w. \tag{7}$$

To show that the cubed root transformation of the wind power (7) retains the TSR characteristics of the standard wind power equation relationship (2), the P_{SA} and standard power equations are plotted together in Fig. 4 where the red solid curve represents the power curve given by (1) for $v_w = 3$ m/s and the red dotted line represents the P_{SA} given by (7) for $v_w = 3$ m/s. Fig. 4 shows that both the standard power curve and modified wind power curves (i.e., P_{SA} curves) yield MPPs at the same λ_{opt}.

Fig. 5 illustrates the SA power curves P_{SA} with the SA linear equivalent of the MPC $P_{\mathrm{SA},\lambda k}$ together with the standard wind power equations and its corresponding MPC. The PSA curves represented as the dotted curves in Fig. 5 and the solid curves represent the standard power curves. With the conventional representation of the MPC, it is difficult to identify the full MPC with a single MPP to facilitate the extrapolation of the MPPs for future wind conditions without knowledge of the

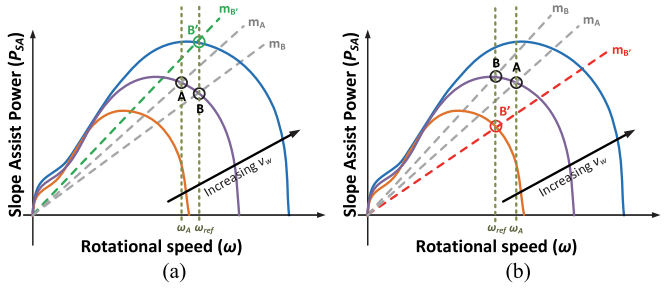

Fig. 6. (a) State observer wind increase detection. (b) State observer wind decrease detection.

system characteristics. However, the SA linear MPC equivalent $P_{\mathrm{SA},\lambda k}$ enables the identification of all the operating points that correspond to a specific point on the system's internal C_p curve [see Fig. 2(a)] and was derived from the general form of the power equation and the TSR relationship. Therefore, the SA methodology allows the determination of a slope value ($m_{\lambda k}$) that represents all the operating points that have the same aerodynamic efficiency (dictated by the C_p value and TSR) without any prior knowledge of the system characteristics or complicated measurements.

B. State Observer

The state observer module monitors, records, and analyzes the system's operation parameters to determine if the system is ready for the next perturbation step and identify whether an atmospheric change has occurred. The observer records the rotational speed, output power, and $m_{\lambda k}$ values to differentiate between legitimate power variations due to intentional operating point perturbations from atmospheric changes and to determine whether the MPPT or PLS module should be active.

The observer determines wind change by using the $m_{\lambda k}$ values. If an increase in the rotational speed results in an increase in $m_{\lambda k}$ value, then an increase in v_w is detected [see Fig. 6(a)]. From Fig. 6(a), it can be seen that if there is no change in wind conditions, an increase in rotational speed (operating point $A \rightarrow B$) will result in a decrease in the slope value ($m_A \rightarrow m_B$ where $m_B < m_A$). However, if there is an increase in v_w and the controller has commanded an increase in rotational speed, the system will move from operating point A to point B′ instead and an increase in the slope value will be observed ($m_A \rightarrow m_{B'}$ where $m_{B'} > m_A$). Similarly, the observer identifies a decrease in v_w if it detects that decrease in the rotational speed has caused the slope value to decrease [see Fig. 6(b)]. Fig. 6(b) illustrates the wind decrease detection; if the wind conditions have not changed, a decrease in rotational speed (operating point $A \rightarrow B$) should result in an increase in the slope value ($m_A \rightarrow m_B$, where $m_B > m_A$).

Depending on the power conditions and feedback from the MPPT and PLS modules, the state observer also decides which module to activate to achieve the highest possible power extraction efficiency while minimizing wasted power. By default, the system is configured to operate in the MPPT mode to extract as much power as possible from the wind. However, if the state

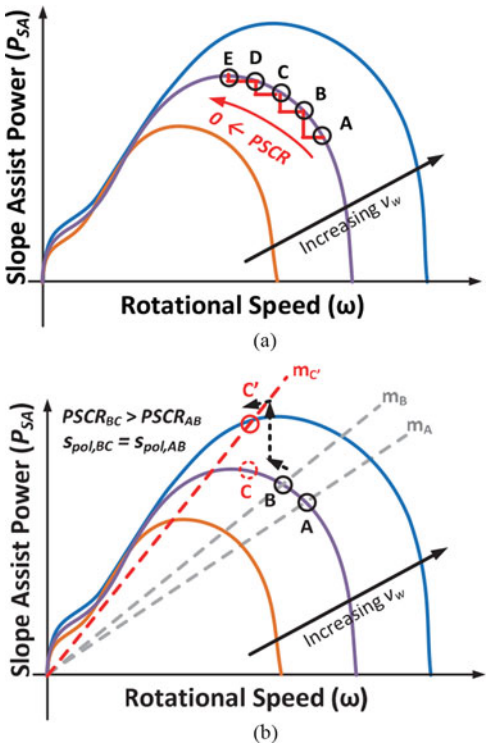

Fig. 7. (a) PSCR gradually decreases toward 0 with no change in wind condition (where PSCR ≈ 0 means at MPP); (b) MPPT module wind detection.

observer detects that the power exceeds that of the predetermined power limit, the PLS module is activated. The transition condition for the controller to transition from the PLS back to MPPT, on the other hand, requires the cooperation between the observer and the PLS module and will be discussed in detail in Section D.

C. SA MPPT

The SA MPPT seeks the MPPs of the system using the slope parameter as a reference for the system's TSR to proactively compensate for the MPP overshoot or wind changes. To minimize the MPP search error, the MPPT algorithm also has a wind change detection feature that complements the observer's wind change mechanism. With no knowledge of the wind turbine characteristics, the MPPT algorithm adapts to wind turbine over time and establishes an approximation of the system's MPC to expedite future MPP searches. The algorithm stores the m_λ values of each determined MPP and calculates an average $m_{\lambda \text{opt}}$ that is used to represent the system's MPC curve. By doing so, the algorithm can adapt to system parameter shifts due to aging and obtain a fairly accurate representation of the MPC by minimizing the effects of any occasional MPP errors.

The MPPT algorithm detects wind change by monitoring the change in power and the change in ω through the power speed change ratio (PSCR) given by (8), where the subscript *n* represents the current time step. If there is no change in the wind condition and the MPPT algorithm operates normally, the PSCR should decrease as the system is moving toward the MPP, where the PSCR $= 0$ [illustrated in Fig. 7(a)]. As such, a wind change is detected when the ratio between the change in power and the change in speed (*PSCR*) increases and there is no change in rotational speed polarity (s_{pol}); the speed polarity is expressed as (9) and s_{change} (10) represents the change in ω. Without wind change, the only exception to a consistently decreasing PSCR is when the system has passed the MPP and is reversing direction toward the MPP where the power would be greater (i.e., s_{pol} has changed). Essentially, s_{pol} is defined to be positive if an increase in ω is commanded, and it is defined to be negative if a decrease in ω is commanded. If there is no change in the wind conditions, a change in s_{pol} only occurs when the algorithm is compensating for overshooting the MPP (i.e., the system has passed the MPP). The MPPT wind change detection is illustrated in Fig. 7(b).

The MPP wind change detection complements the observer's wind change detection. Recall from the previous section that the observer detects wind change when both ω and $m_{\lambda k}$ decrease or increase. Therefore, the wind change condition illustrated in Fig. 7(b) would not be detected by the observer module since a ω decrease (from operating point B to C′) caused an increase in the slope value ($m_{C'} > m_B$). Due to the different operating model of the MPPT and PLS, the MPPT wind detection is not applicable to PLS module and, therefore, is not integrated in the observer (see Section D)

$$\text{PSCR} = abs\left(\frac{P_n - P_{n-1}}{\omega_n - \omega_{n-1}}\right) \tag{8}$$

$$s_{\text{pol}} = \begin{cases} 1, & \text{if } s_{\text{change}} \geq 0 \\ 0, & \text{if } s_{\text{change}} < 0 \end{cases} \tag{9}$$

$$s_{\text{change}} = \frac{\omega_n - \omega_{n-1}}{\omega_{n-1}}. \tag{10}$$

The main difference between the SA MPPT and the conventional P&O MPPT logic is that it uses pTSR values to reduce the MPP convergence rate, minimize oscillation around the MPP, and mitigate decision errors due to atmospheric change. The SA achieves this by using the pTSR values to extrapolate MPPs for a wide range of wind conditions and by using pTSR as a reference point in the event of a power decrease. When there is no atmospheric change present and a decrease in power is observed (caused by passing the MPP), the algorithm can identify the operating range where the MPP is located and move back toward the last operating state (denoted by the last pTSR value) while minimizing overcompensation (i.e., passing the last operating state)—thereby reducing oscillation around the MPP (see Fig. 8). The pTSR also allows the MPPT algorithm to resume its MPP search process in the event of any atmospheric change. Fig. 9 illustrates the SA process when wind changes are identified by the observer or MPPT modules. In Fig. 9, the algorithm drives the WES toward a new operating point that corresponds to the previous pTSR value m_G (derived from the previous wind condition, operating point G) when atmospheric change is detected. The algorithm is able to identify a pTSR value to represent the last known operating state (prior to the interruption) for the new wind condition and resume the MPP search from where it left off. By using the pTSR values, the proposed MPPT algorithm alleviates the MPP oscillation problem and logical error vulnerability due to atmospheric changes seen in conventional HCS MPPT algorithms.

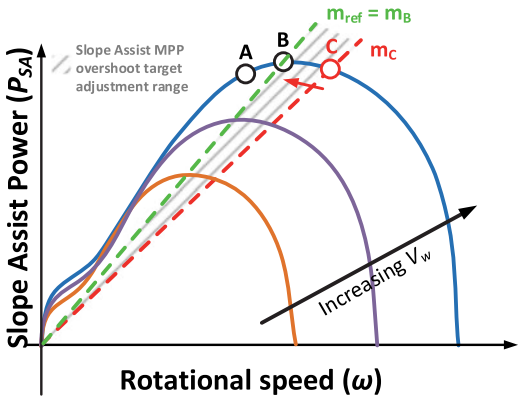

Fig. 8. MPPT module's MPP overshoot adjustment range. Decrease in power ($B \rightarrow C$) is detected and no wind change has been identified: SA activated with the slope reference as m_{ref}.

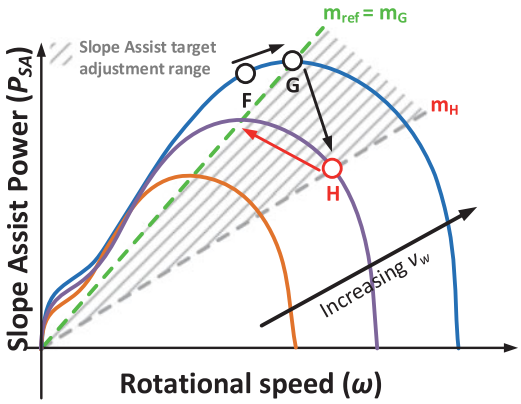

Fig. 9. MPPT SA adjustment in the event of wind change.

The MPP search in the training mode begins by receiving the steady-state signal from the state observer. With the signal received, the training module calculates the current slope m_c as per (5); percent difference from the ω_{ref} and ω_n as given by (11); percent power change between current and prior operating point (P_{change}) as given by (12); percent ω change between current and prior operating point (s_{change}) as given by (10); and speed change polarity (s_{pol}) as given by (9)

$$s_e = \frac{\omega_n - \omega_{\text{ref}}}{\omega_{\text{ref}}} \tag{11}$$

$$P_{\text{change}} = \frac{P_n - P_{n-1}}{P_{n-1}}. \tag{12}$$

If s_e is almost zero (i.e., less than ε_{se}), then the system has reached the speed reference and the algorithm calculates the PSCR according to (8) to detect any changes in the wind conditions during the transition between the previous and current operating point. Essentially, the algorithm perturbs the system based on the measured (P and ω) and calculated ($m_{\lambda k}$, s_e, P_{change}, s_{change}, s_{pol}, and *PSCR*) parameters and observes the resulting system behavior.

The operating principles of the proposed MPPT algorithm are summarized as follows:

If $P_{\text{change}} > \varepsilon_{P,\text{MPP}}$ and *no wind changes* [illustrated in Fig. 10(a)]

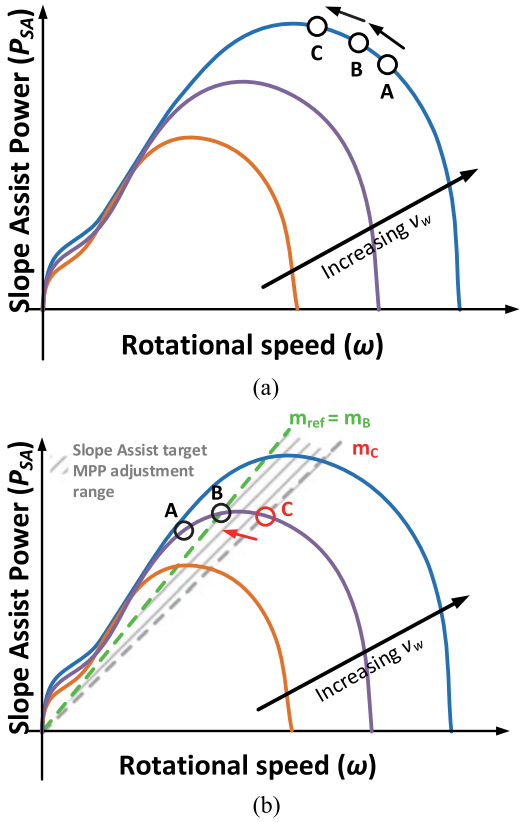

Fig. 10. MPPT operating principle. (a) $P_{\text{change}} > 0$ and no wind change condition; (b) $P_{\text{change}} < 0$ and/or wind change SA condition.

1) continue to change the speed reference with the same polarity, where $\Delta\omega_{\text{ref}} \alpha P_{\text{change}}$.
   If $P_{\text{change}} < -\varepsilon_{P,\text{MPP}}$ and/or wind changes [illustrated in Fig. 10(b)].
2) *MPP overshoot or wind change has occurred* so *guide* the system back to its last known operating TSR state using the last $m_{\lambda k}$ value as a reference. Recall that since each $m_{\lambda k}$ represents a unique TSR value, the slope value represents the universal position (that has the same corresponding TSR and C_p value) on all the power curves (regardless of v_w).

Due to the shape of the power curves, the speed reference calculations differ depending on whether the current $m_{\lambda k}$ value is greater or less than the m_{ref} to minimize the number of perturbation steps to converge the slope reference. The SA ω_{ref} equation is given by (13) where $P_{\text{SA}} = \sqrt[3]{P}$ and the calculation process is illustrated by Fig. 11

$$\omega_{\text{ref}} = \begin{cases} \dfrac{P_{\text{SA}}}{m_{\text{ref}}}, & \text{if } m_\lambda > m_{\text{ref}} \\ \dfrac{1}{2}\left(\omega + \dfrac{P_{\text{SA}}}{m_{\text{ref}}}\right), & \text{if } m_\lambda < m_{\text{ref}}. \end{cases} \tag{13}$$

By using the slope values as its guide, the algorithm drives the system toward its previous "state" rather than its previous operating point to resume the search process from where it left off. Since the algorithm evaluates the changes in both the pTSR and P_{change} rather than just the power change alone, the

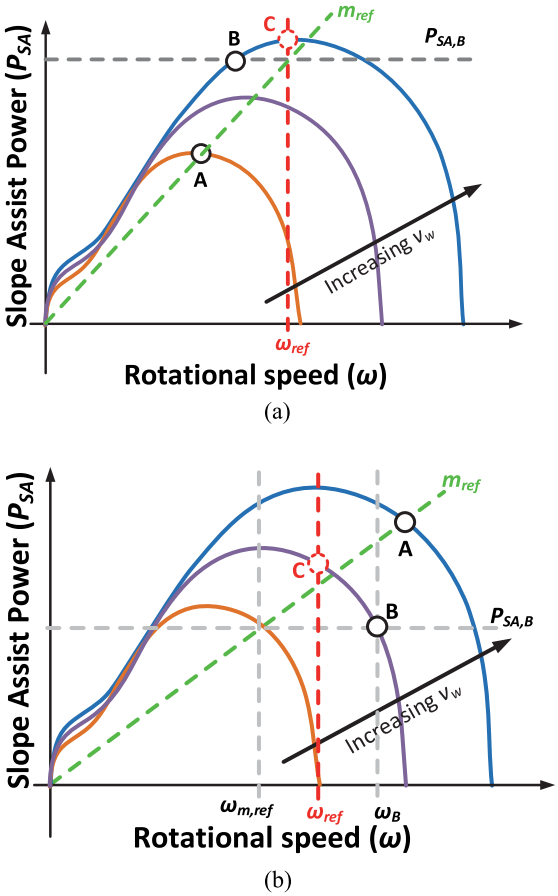

Fig. 11. SA $\omega_{\rm ref}$ calculation process. (a) $m_B > m_{\rm ref}$ scenario where $\omega_{\rm ref} = P_{{\rm SA},B}/m_{\rm ref}$. (b) $m_B < m_{\rm ref}$ scenario where $\omega_{\rm ref} = 0.5[\omega_{\rm ref} + (P_{{\rm SA},B}/m_{\rm ref})]$.

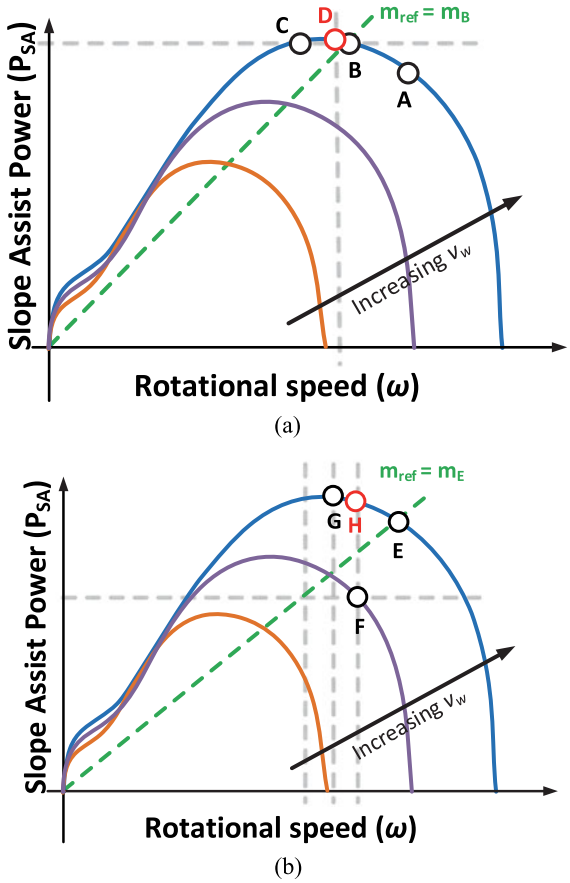

Fig. 12. MPPT SA special cases. (a) Case (a): MPP is found during SA convergence; (b) Case (b): MPP divergence, and (c) reversal of $s_{\rm pol}$.

algorithm is able to detect wind speed changes, and therefore, robust with respect to frequent atmospheric changes. It is important to mention that during the slope convergence, the algorithm checks for the following:

a) If the MPP has been found (i.e., if (14) is satisfied where $\varepsilon_{p,{\rm MPP}}$ is the acceptable error threshold for the $P_{\rm change}$ to be considered almost zero)

$$|P_{\rm change}| \leq \varepsilon_{p,{\rm MPP}}. \tag{14}$$

b) If the system is moving away from the MPP ($P_{\rm change} < -\varepsilon_{P,{\rm MPP}}$). Going toward the MPP should always yield $P_{\rm change} > \varepsilon_{P,{\rm MPP}}$ when there is no wind change.

c) If the new calculated speed adjustment dictates a change in the direction of movement, $s_{\rm pol}$.

If cases a) or b) is detected, the algorithm will halt the slope convergence process. In case a), the MPP has been found during slope convergence mode so the algorithm will register the MPP in the database and refrain from any further speed adjustments until $P_{\rm change} > \varepsilon_{p,{\rm MPP}}$ (which occurs only if the atmospheric conditions change). Fig. 12(a) illustrates case a) where the system is moving toward $m_{\rm ref}$ (the slope value of point B) from point C and the MPPT halts the slope convergence process at point D where $P_{\rm change} \leq \varepsilon_{p,{\rm MPP}}$. In case b), the algorithm has detected that the current $m_{\rm ref}$ is causing the system to move away from the MPP (this scenario is illustrated in Fig. 12(b) where the MPPT halts the slope convergence process at point H). As a result, the algorithm activates SA and replaces the slope reference with the slope of the previous operating point to return to the previous operating state [point G in Fig. 12(b)]. When case c) is detected, the algorithm continues with the slope convergence process but commands a small speed adjustment to probe the system. Case c) is illustrated in Fig. 12(b) where the MPPT commanded the ω to increase (from G toward $m_{\rm ref}$) instead of continuing to decrease (point F to G). This is done to prevent the system from potentially moving too far from the MPP due to a wind change and a nonoptimal slope reference where the system is trying to move toward $m_{\rm ref1}$). Since the algorithm was previously decreasing ω, the algorithm does not immediately command a large increase in ω to move toward $m_{\rm ref1}$. Rather, the algorithm demands a small change (to point E) to probe the system.

D. Power Limit Search

The proposed PLS algorithm is a modified version of the SA MPPT method; employing a similar search methodology, the PLS searches for the operating points that will result in the desired output power level rather than the MPP. The PLS identifies and maintains the *pTSR* that results in the target power level with the assistance of the wind change state observer module.

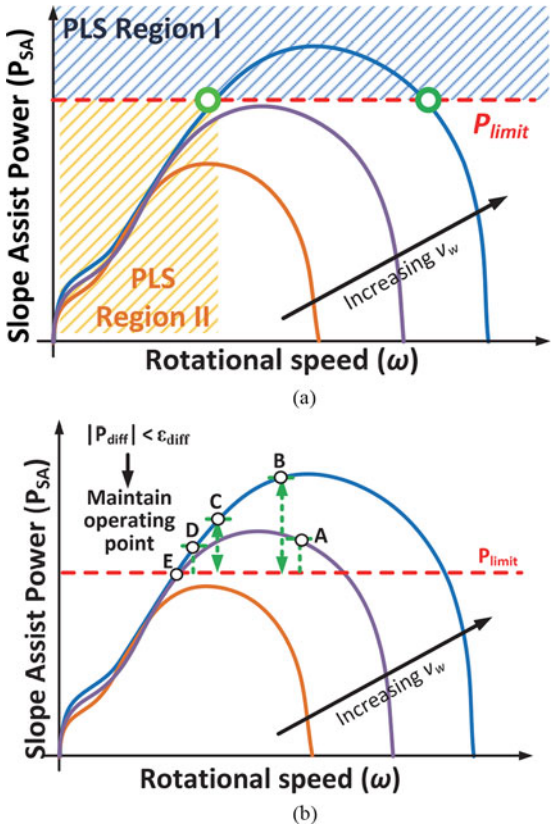

Fig. 13. PLS Operation. (a) PLS operating regions; (b) PLS basic operating principle.

The PLS is activated when the controller is operating in MPPT mode and the observer has identified that the system is generating more power than the defined power limit (P_{limit}); the PLS operating region is highlighted in the shaded areas in Fig. 13(a). While the PLS region I in Fig. 13(a) is the primary operating region where the measured power is higher than the power limit, the system may briefly operate below the power limit (PLS region II) while the PLS is searching for the power target operating point. Together with the observer module, the PLS uses the pTSR value to determine when to correctly transition back to the MPPT mode.

Due to the near parabolic shape of the power curves, there exists two operating points that result in the target power value for each wind speed [see (15) and Fig. 13(a)]. To minimize the WES mechanical stress and avoid over speeding the WES generator, the proposed PLS methodology has been designed to seek the operating points that achieve the target power generation at the lowest possible generator speed (16). As illustrated in Fig. 13(b), to locate the lowest generator speed that results in the target power, the PLS module will reduce ω in proportion to the power difference (P_{diff}) as given by (17), where P_{diff} is expressed as (18) and K is a proportional constant. The PLS will continue to decrease ω until P_{diff} is sufficiently small (i.e., $P_{\text{diff}} < \varepsilon_{p\text{diff}}$) or if the system output power is below the power limit (i.e., $P_{\text{diff}} < -\varepsilon_{p\text{diff}}$). The proportional constant K dictates the perturbation step size of the PLS module. Similar to the step-size selection in HCS algorithms, K is generally selected to be a value between 0.05 and 0.1 to balance the tradeoff between the power limit accuracy (small K) and the convergence time (large K).

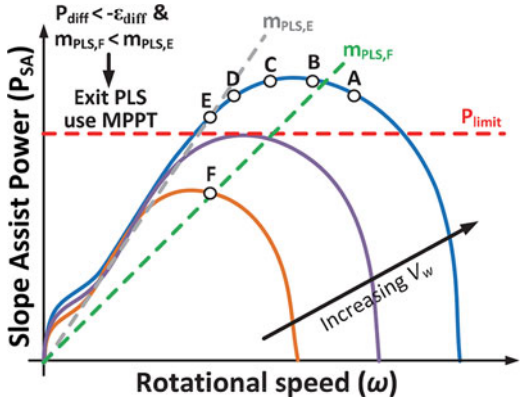

Fig. 14. PLS exit condition.

Once the PLS is active, it signifies that the system is generating a surplus of power and that the system should decrease ω to reduce the power output. Therefore, unlike the MPPT module, the PLS is not affected by increases in wind and will continue to decrease ω with respect to (17) regardless of the increased power [see Fig. 13(b)]. The PLS only requires the identification of wind decreases which can potentially cause the output power decrease below the target power limit

$$P_{\text{limit}}(\omega_1) = P_{\text{limit}}(\omega_2), \quad \text{where } \omega_2 > \omega_1 \tag{15}$$

$$\omega_{\text{target}} = \min\{\omega_2, \omega_1\} \tag{16}$$

$$\omega_{\text{ref},n+1} = \omega_{\text{ref},n}((1 - K(P_{\text{diff}})) \tag{17}$$

$$P_{\text{diff}} = \frac{P - P_{\text{limit}}}{P_{\text{limit}}}. \tag{18}$$

Once the controller acknowledges that the measured power has dropped below the power limit in the PLS mode, there are two possible scenarios: 1) the WES has passed the target operating point due to normal adjustment and no atmospheric change has occurred (PLS Region II); 2) the wind speed or air density has decreased (possible exit PLS condition). In case 1), the WES is close to the target operating point, so the controller will continue to adjust the WES's operating point with respect to (17). In case 2), the observer will activate the MPPT mode if it has identified a decrease in wind speed or air density through its wind change detection scheme (see Fig. 14); recall that the state observer defines a wind decrease when $\omega_n < \omega_{n-1}$ and $m_{\lambda k,n} < m_{\lambda k,n-1}$.

III. Results and Performance of the Proposed Power Management Controller

In order to verify the functionality of the proposed controller, the WES shown in Fig. 1 is simulated in PSIM 9.3, with the system parameters given in Table I.

A. Simulation Results

In the simulation studies, the power management controller was subjected to a wide variety of atmospheric conditions. The WES model used in the simulation studies is illustrated by

TABLE I
SYSTEM PARAMETERS

Boost converter parameters	
L_b	1.5 mH
f_s	20 kHz
C_b	200 μF
V_o	400 V
PMSG and turbine parameters	
Rated Power	3 kW
Air density (ρ)	1.225 kg/m^3
PMSG Inertia (J)	0.0527 kg.m^2
Cut-in wind speed	3 m/s
Rated wind speed	12 m/s
Radius (R)	1.86 m
Number of poles (N_p)	14
Gearbox	1:1

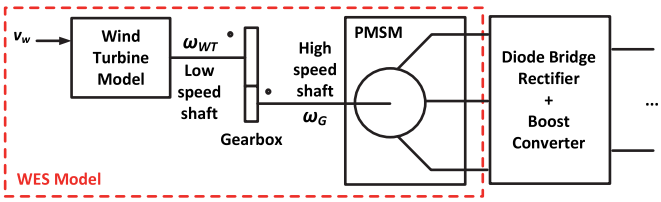

Fig. 15. WES model created in PSIM.

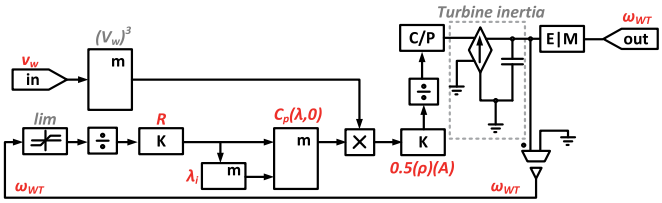

Fig. 16. Wind turbine model created in PSIM.

Figs. 15 and 16 is the wind turbine model created in PSIM. The C_p function used in the simulation study was based on the relationship from the wind turbine model provided by MATLAB Simulink [27]. The turbine model is described by (16) and (20), where the coefficients $c_1 = 0.5176$, $c_2 = 116$, $c_3 = 0.4$, $c_4 = 5$, $c_5 = 21$, $c_6 = 0.0068$. In Fig. 16, the input of the wind turbine model is the wind speed v_w, and the output is the mechanical turbine shaft speed ω_{WT}.

To quantify the effectiveness and robustness of the SA MPPT, its performance was compared to the standard fixed and variable speed P&O algorithms under identical atmospheric conditions ($v_w = 7 - 9.5$ m/s and $\rho = 1.225$ kg/m^2). In this comparison, the P&O algorithms employ the same steady-state detection method as the proposed algorithm to properly show the effectiveness of their respective algorithm logic without bias, provided that the system's ideal dimensionless TSR value in this example is 8.1 and the corresponding ideal m value used in the proposed MPPT control method is 0.0354. The three algorithms (fixed-step size, variable-step size, and the proposed SA MPPT) were subjected to the same wind profile

$$\lambda_i = \frac{1}{\lambda + 0.08\beta} - \frac{0.035}{\beta^3 + 1} \tag{19}$$

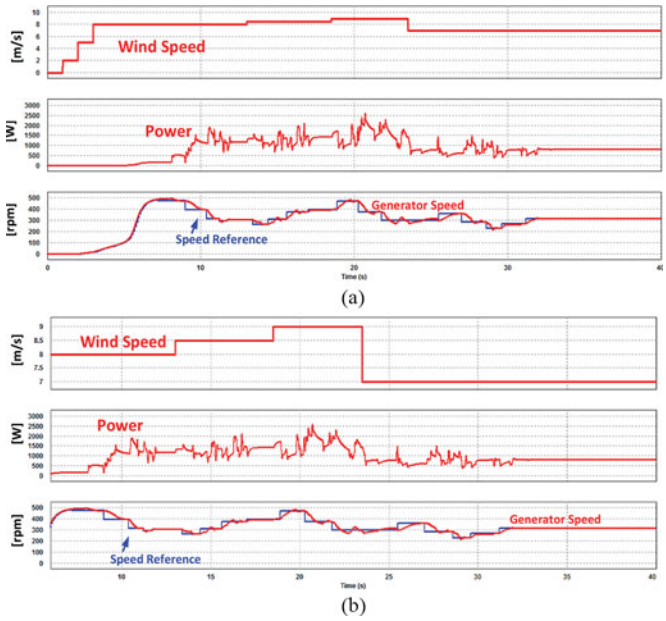

Fig. 17. Performance of the standard fixed-step size P&O algorithm (average power captured = 1066 W).

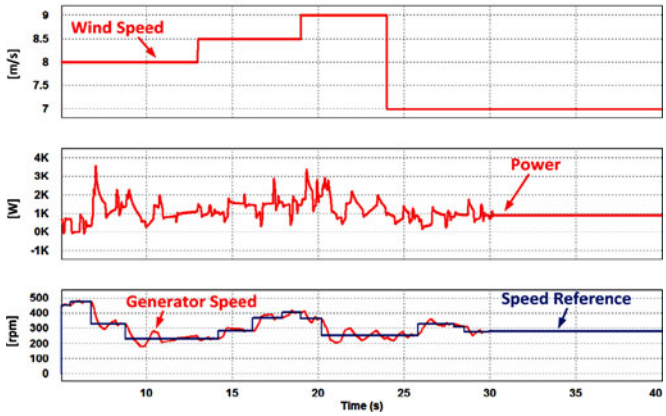

Fig. 18. Performance of the standard variable-step size P&O algorithm (average power captured = 1106 W).

$$C_p(\lambda,\beta) = c_1\left(\frac{c_2}{\lambda_i} - c_3\beta - c_4\right)e^{\frac{-c_5}{\lambda_i}} + c_6\lambda. \tag{20}$$

The wind profile used in the comparison featured gradually increasing wind speeds and a sharp decrease in wind; the wind speed varied from 7 to 9 m/s. Figs. 17–19 illustrate the performance of the fixed-step size P&O, variable-step size P&O, and the SA algorithms, respectively, for this wind profile. In this scenario, the P&O algorithms performed fairly well and were able to obtain the system's MPPs in most cases. However, the SA MPPT was able to efficiently identify all the MPPs and was able to extract 16% more power from the wind than the standard fixed-step size P&O algorithm and 12% more power than the variable-step size P&O algorithm (see Table II). The power coefficient performances of these algorithms are summarized in Fig. 20. Given that the optimal power coefficient value of the wind system is 0.47, the SA MPPT was achieved a higher

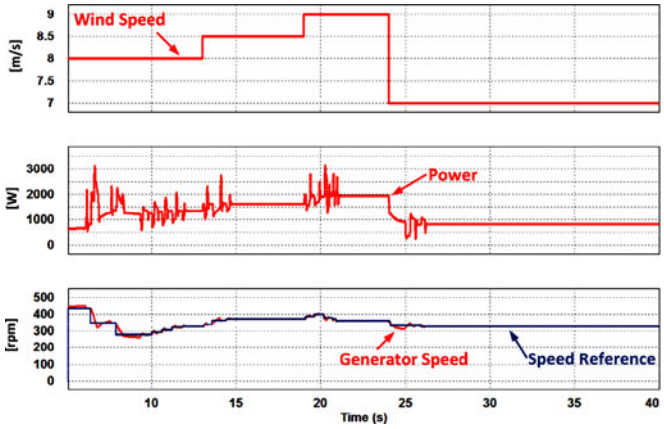

Fig. 19. Performance of the SA MPPT algorithm (1238 W).

TABLE II
PERFORMANCE OF THE FIXED-STEP SIZE P&O, VARIABLE-STEP SIZE P&O, AND SA MPPT

MPPT Method	Fixed-step size P&O	Variable-step size P&O	SA MPPT
Average Power [W]	1066	1106	1238

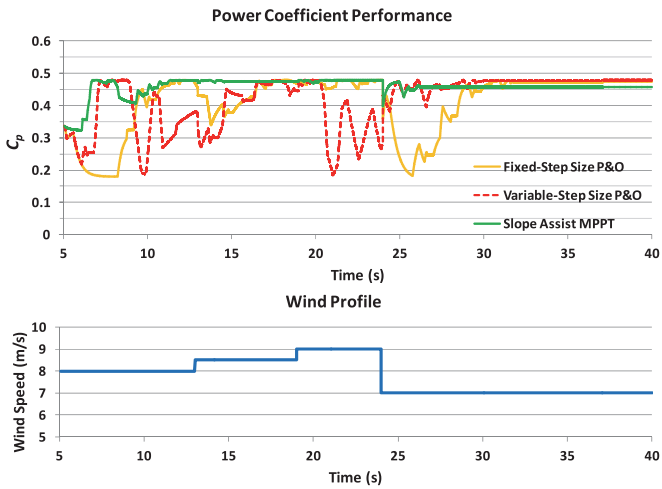

Fig. 20. Power coefficient performance of the fixed-step size P&O, variable-step size P&O, and the SA MPPT (comparison performed under atmospheric identical conditions as depicted in Fig. 20).

average C_p value than the conventional algorithms. The SA MPPT achieved an average C_p value of 0.46, while the fixed- and variable-step P&O algorithms achieved average C_p values of 0.41 and 0.42, respectively.

Fig. 27 illustrates the automatic transitioning between the MPPT and PLS modes. At startup, the MPPT is active for $v_w = 8$ m/s and continues to be active when the wind speed changes to 8.5 m/s. At $v_w = 8$ m/s, the algorithm achieved a TSR value of 8 before the wind changed to 8.5 m/s. After detecting an increase in wind speed at 12.5 s ($v_w = 8.5$ m/s), the algorithm quickly sought out the MPP for the new wind speed and was to operate at the optimal TSR value of 8.1. At 19 s, the algorithm successfully detects an increase in wind speed to 9 m/s and that the WES is generating surplus power. Due to the surplus

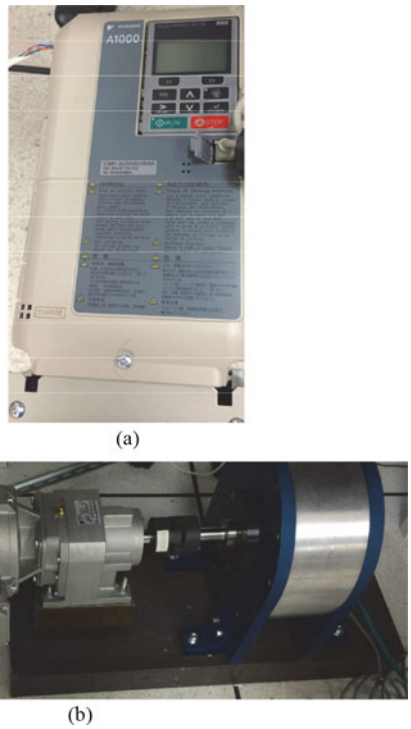

(a)

(b)

Fig. 21. (a) Yaskawa A1000 motor drive; (b) PM generator set.

power, the power management control activated the PLS and successfully regulated the output power to the set power limit of 1600 W. As a result, the WES operated at a suboptimal operating point with a TSR value of 6.4 until it detected a decrease in wind speed at 24 s. At 24 s, the algorithm detected that the wind speed has decreased and that the power has dropped below the power limit. As a result, the algorithm transitioned back to the MPPT mode and successfully resumed operation at a near optimal TSR value of 7.9 at 27 s. Simulation results that show the energy captured by the proposed method and the conventional P&O method on a 3-kW system have been provided as shown in Fig. 28. The results were obtained based on a 90 s variable wind speed profile. Fig. 28 showed that under the same wind profile, the proposed method is able to capture 12.2-kJ energy more than the conventional variable-step P&O technique.

B. Experimental Results

Experimental works were performed to further support the features of the proposed energy management control scheme, as well as the simulation results. The experimental setup consists of a 200-W boost power converter with a three-phase-diode bridge rectifier, a wind turbine simulator, and a DSP MPPT controller. The wind turbine simulator is comprised of a Nord SK112MH/4 induction motor, a Nord 4.66:1 gearbox, a Yaskawa A1000 motor driver as shown in Fig. 21(a), and an ALXION 300STK2M permanent magnet (PM) synchronous generator as shown in Fig. 21(b).

Fig. 22 shows a picture of the final experimental setup. In the experimental setup, the Yaskawa A1000 is only used to control the induction motor. The wind turbine simulator

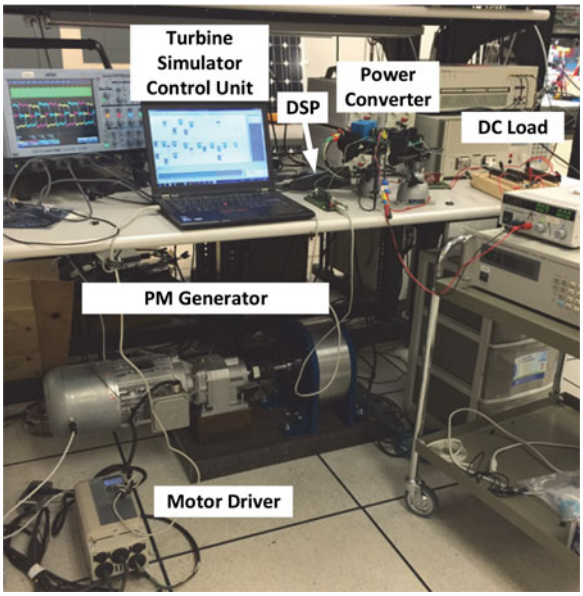

Fig. 22. Experimental setup in the laboratory.

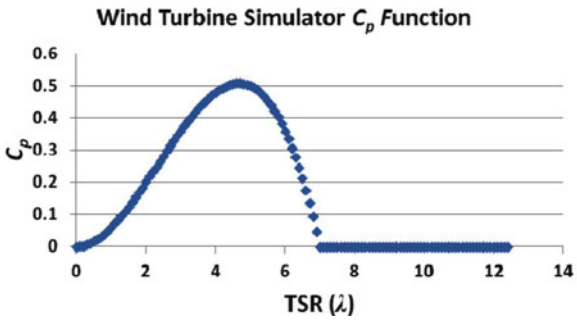

Fig. 23. C_p curve created in the wind turbine simulator model.

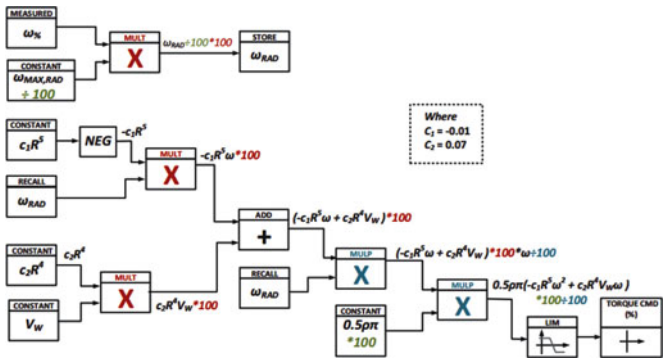

Fig. 24. Wind turbine simulator program implemented in the Yaskawa A1000 induction motor driver using the DriveWorks EZ software.

program was implemented in the Yaskawa A1000 driver using the DriveWorks EZ software. Using the DriveWorks EZ software, the C_p characteristic was first created as shown in Fig. 23, then the torque characteristic was programmed into the Yaskawa induction motor driver. Fig. 24 shows the complete block diagram of the wind turbine simulator implemented in in the Yaskawa A1000 induction motor driver using the DriveWorks EZ software. To verify the functionality of the turbine

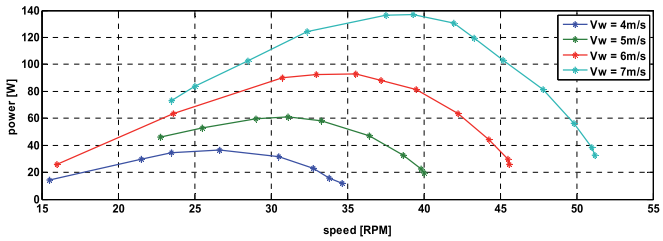

Fig. 25. Measured power curves of the wind turbine simulator setup (power versus speed).

TABLE III
WIND ENERGY SYSTEM PARAMETERS (EXPERIMENTAL PROTOTYPE)

Boost converter parameters	
L_b	2.2 mH
f_s	20 kHz
C_b	200 μF
V_o	100 V
Machine parameters	
Rated Power	200 W
Air density (ρ)	1.225 kg/m^3
PMSG Inertia (J)	0.0527 kg·m^2
Induction machine inertia (J)	0.0128 kg·m^2
Cut-in wind speed	3 m/s
Rated wind speed	8 m/s
Radius (R)	1.5 m
Number of poles (N_p)	24
Gearbox	4.66:1

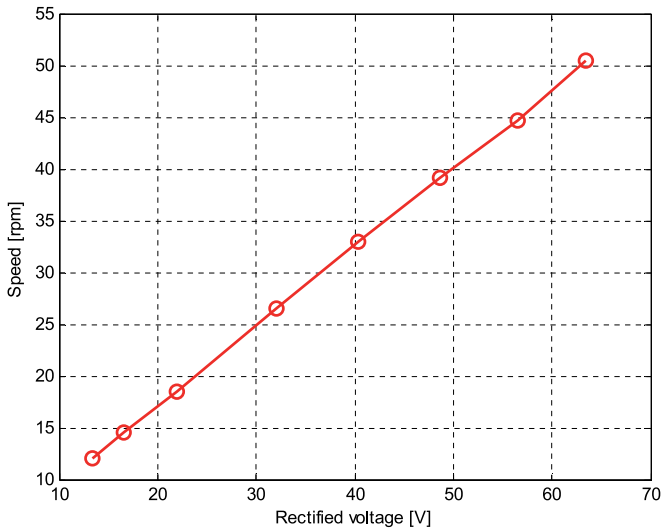

Fig. 26. Measured speed versus rectified voltage in the experimental setup.

simulator, the system was subjected to varying load conditions for a range of wind speeds. Fig. 25 illustrates the system's experimentally obtained power characteristics. The system and boost converter circuit parameters for the experimental setup are given in Table III.

In the setup, it has been verified that the rectified voltage is directly proportional to the rotational speed of the generator. A plot that displays the relationship between the measured speed and the rectified voltage has been added as shown in Fig. 28. The

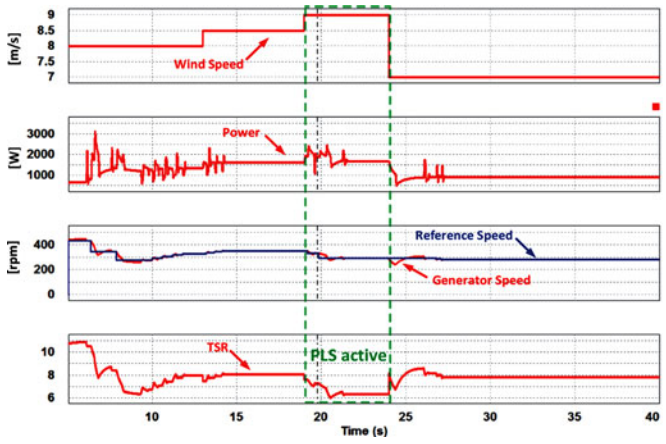

Fig. 27. Performance of the power management controller with active PLS ($P_{\text{limit}} = 1600$ W). MPPT active at $v_w = 7 - 8.5$ m/s and PLS active at $v_w = 9$ m/s.

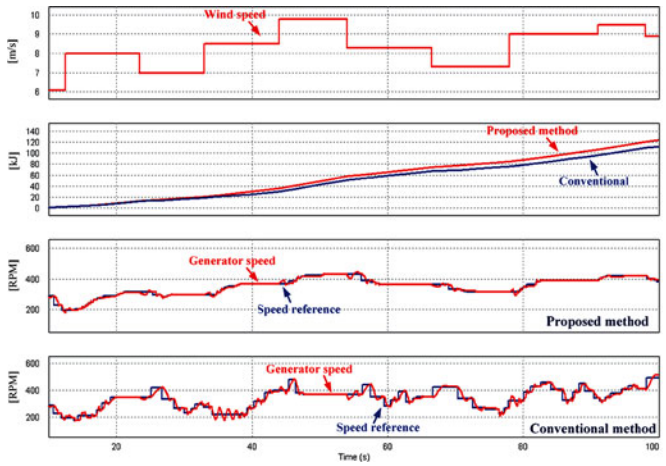

Fig. 28. Energy capture comparison between the proposed method and the conventional P&O method.

plot shows that the measured speed and rectified voltage exhibit an almost linear relationship. Hence, in the experimental setup, instead of using a speed sensor to obtain the rotational speed, the rectified voltage is fed to the converter controller to indirectly control the rotational speed. Using the wind turbine simulator, the performance of the fixed-step and variable-step P&O algorithms were compared with the proposed SA MPPT algorithm. The MPPT algorithms were subjected to the same wind conditions and the wind speed was changed when the algorithm found the MPP. Each algorithm was subjected to three wind speeds (6, 5, and 4 m/s); the wind speed change occurred after a successful MPP search. Figs. 29 and 30 show the MPPT performance with the fixed-step and variable-step P&O algorithms, respectively. The MPP values obtained by all the algorithms were the same, but the fixed-step P&O had the longest search times, while the proposed SA had the shortest. Figs. 31 and 32 show the MPPT performance with the proposed SA MPPT control method. The MPP search times for the algorithms are summarized in Table IV. It is observed that the average MPP search time for the proposed SA MPPT algorithm is significantly shorter;

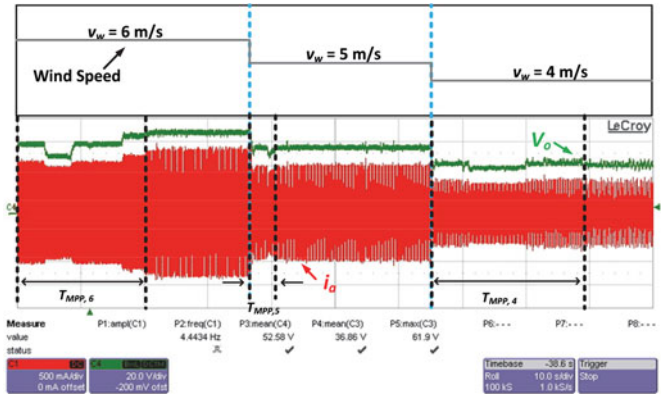

Fig. 29. Fixed-step P&O algorithm performance (output voltage (V_o): 20 V/div; generator per-phase output current (i_a): 0.5 A/div).

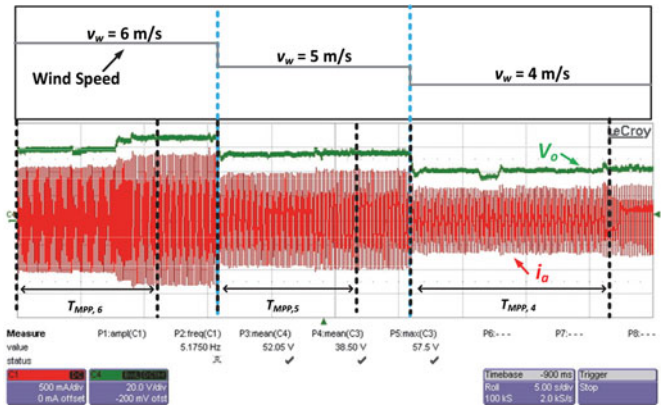

Fig. 30. Variable-step P&O algorithm performance (output voltage (V_o): 20V/div; generator per-phase output current (i_a): 0.5A/div)

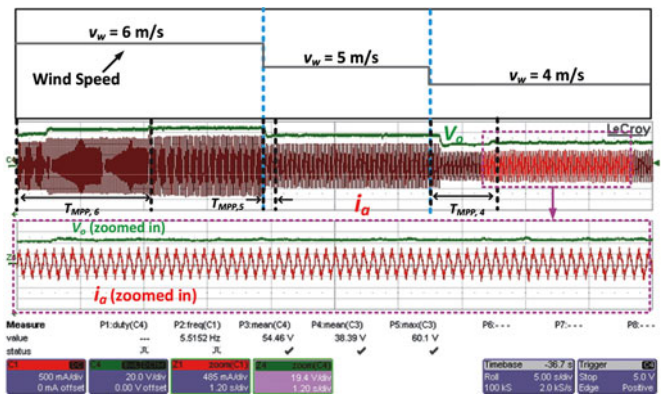

Fig. 31. SA MPPT algorithm performance. Bottom graph is the zoomed in portion of the output voltage and phase current (output voltage (V_o): 20 V/div; generator per-phase output current (i_a): 0.5 A/div; V_o (zoomed in): 19.4 V/div; i_a (zoomed in): 0.485 A/div).

the proposed algorithm achieved an average MPP search time of 6.7 s. The proposed algorithm was, on average, 58% faster than the fixed-step P&O and 47% faster than the variable-step P&O at determining the MPPs.

The functionality of the power management controller (which consists of the SA MPPT and PLS) was also experimentally verified. Fig. 33 illustrates that the controller seamlessly switches

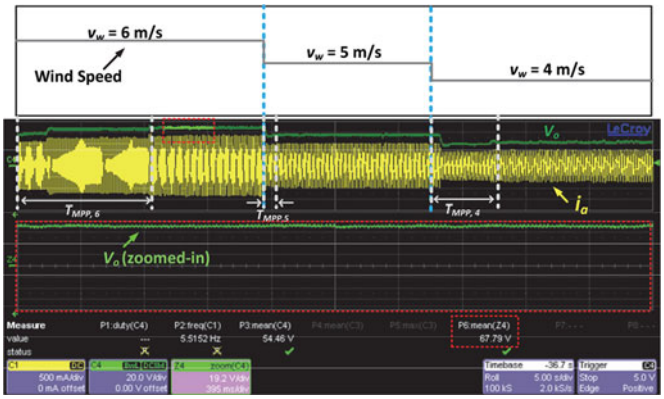

Fig. 32. SA MPPT algorithm performance: zoomed in at MPP for $v_w = 6$ m/s (output voltage (V_o): 20 V/div; generator per-phase output current (i_a): 0.5 A/div; V_o (zoomed in): 19.2 V/div).

TABLE IV
MPP SEARCH TIME COMPARISON

	MPP Search Times (s)			Average Search Time (s)
Algorithm	**v_w = 6 m/s**	**v_w = 5 m/s**	**v_w = 4 m/s**	
Variable-Step P&O	13 s	13 s	15 s	13.3s
Slope Assist	11 s	2 s	6 s	6.7s

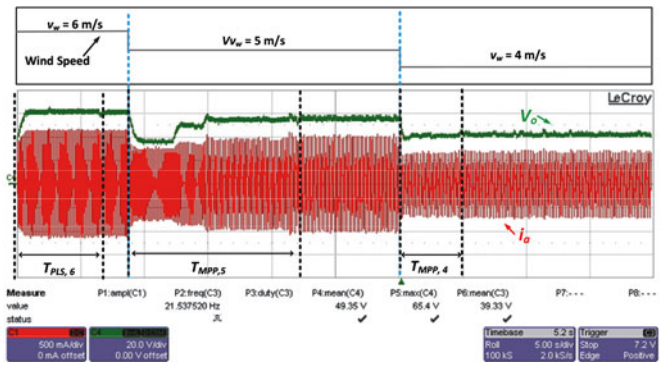

Fig. 33. Proposed power management controller: PLS active at $v_w = 6$ m/s and normal SA MPPT active at $v_w = 4 - 5$ m/s (output voltage (V_o): 20 V/div; generator per-phase output current (i_a): 0.5 A/div).

between PLS and SA MPPT. With the output power limit set at 75 W, the power management controller activated the PLS when subjected to a wind speed was 6 m/s. As Fig. 32 shows, the wind turbine should generate approximately 93 W at the MPP for a wind speed of 6 m/s. Fig. 34 demonstrates that PLS is active, which shows that the output voltage was regulated at approximately 61.1 V, which corresponds to 74.6 W (within 2% of the power limit) rather than reaching the MPP. When the wind speed drops to 5 m/s, the algorithm acknowledged a decrease in wind speed and the power management controller transitioned from the PLS mode to the SA MPPT. Once the controller is in the MPPT mode, the MPPT algorithm promptly identifies the MPP for $v_w = 5$ m/s (where $V_o = 55.6$ V and $P = 62$ W) within 14 s (see Fig. 35). When the wind speed drops further to 4 m/s, the MPPT subsequently acquires the MPP, where $V_o =$

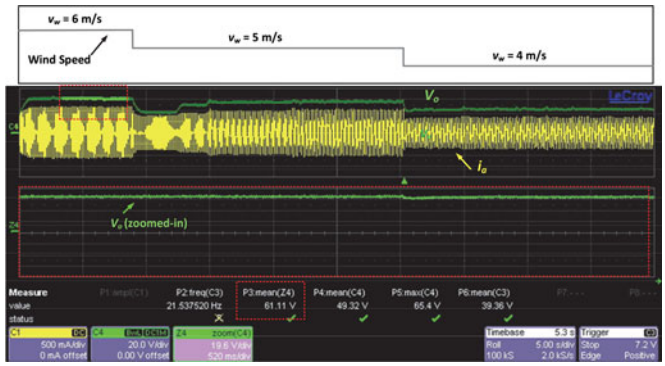

Fig. 34. Proposed power management controller: PLS active at $v_w = 6$ m/s and normal SA MPPT active at $v_w = 4 - 5$ m/s. Zoomed in at $v_w = 6$ m/s (output voltage (V_o): 20 V/div; generator per-phase output current (i_a): 0.5 A/div; V_o (zoomed in): 19.6 V/div).

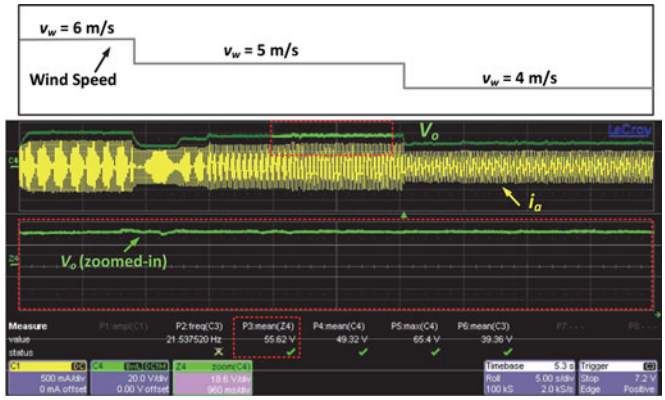

Fig. 35. Proposed power management controller: PLS active at $v_w = 6$ m/s and normal SA MPPT active at $v_w = 4 - 5$ m/s. Zoomed in at $v_w = 5$ m/s (output voltage (V_o): 20 V/div; generator per-phase output current (i_a): 0.5 A/div; V_o (zoomed in): 18.6 V/div).

42.1 V and $P = 35$ W within 5 s as shown in Fig. 36. Table V summarizes the PLS and MPPT performance with respect to the changes in the wind speed. It shows that the calculated and measured values are very close to each other.

C. Comparison of the Proposed MPPT Scheme to Modern MPPT Algorithms

In the recent years, there have been a number of algorithms [7], [12], [13], [19] that have been developed to increase the power extraction efficiency of wind turbines. These algorithms represent a variety of modern MPPT schemes that have been recently presented. The algorithm in [7] achieves high power extraction efficiency and is robust to atmospheric changes since it uses a predetermined control coefficient to represent the wind turbine's internal optimal power–torque characteristic. Unfortunately, due to machine aging, the performance of the algorithm presented in [7] will deteriorate over time since it does not have the means to update the predetermined control coefficient to adapt to the wind system. The P&O algorithm is still highly favored, and many researchers seek different ways to implement it. While the standard P&O algorithm requires generator speed measurement, the algorithm in [12] is a sensorless version that uses the output

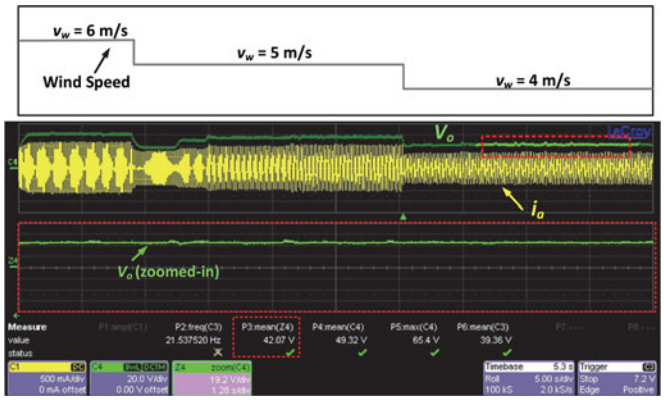

Fig. 36. Proposed power management controller: PLS active at $v_w = 6$ m/s and normal SA MPPT active at $v_w = 4 - 5$ m/s. Zoomed in at $v_w = 4$ m/s (output voltage (V_o): 20 V/div; generator per-phase output current (i_a): 0.5 A/div; V_o (zoomed in): 19.2 V/div).

power and generator terminal voltage (in the place of the generator speed) are used as the input signals. Since the standard P&O algorithms suffer from redundant MPP searches for reoccurring atmospheric conditions and long MPP search times, various enhanced P&O algorithms like in [13] has been proposed. The algorithm uses a modified version of P&O to determine a representation of the system's MPC by observing and determining the region that system is most likely in by storing and analyzing the perturbation decisions and outcomes. If the last *n* perturbations have mostly resulted in a decrease in voltage, then the system is currently operating at the right of the MPP. Otherwise, if the last *n* perturbations have mostly been an increase in voltage, then the system is operating at the left of the MPP. This region determination process only occurs after *n* perturbations have been made with the classic P&O scheme. However, as the authors state that the accuracy of the region determination process is a tradeoff with the MPC search speed since region definition process is dependent on the accuracy of the original P&O algorithm (i.e., smaller perturbation datasets mean that the P&O errors will be prominent and the region determination process will not be effective and a larger dataset will minimize the MPP errors but results in a much longer MPP search process). Chun *et al.* [19] proposed a reinforcement learning technique (called "Q-learning") that uses artificial neural networks to assign reward values (or weights) to the algorithms decisions. The algorithm will choose the "action" (i.e., increase or decrease the rotor speed) that has the highest reward value for the given operating state. The operating state is defined by the rotor speed and the measured power and the reward value awarded to each "action" is determined by the P&O principle. If there is an increase in power = reward value 1, no change in power = reward value 0.5, and decrease in power = reward value 0. While the algorithm is robust to atmospheric change, the algorithm described in [19] requires a large database to store the preferred "actions" for each operating state, has high complexity, and has a long MPP convergence time.

In general, the MPPT performance comparison among the standard P&O, variable P&O, and the proposed method have been illustrated in Figs. 30–33. Table VI is a qualitative comparison between a variety of the state-of-the-art MPPT algorithms [7], [12], [13], [19] and the proposed method.

TABLE V
EXPERIMENTAL PERFORMANCE SUMMARY WITH PLS AT $v_w = 6$ M/S AND MPPT AT $v_w = 5$ AND 4 M/S WITH THE PROPOSED CONTROL METHOD

	Average output voltage		
v_w	*6m/s*	*5m/s*	*4m/s*
Calculated value	61V	55V	42V
Measured value	**61.11V**	**55.62V**	**42.07V**

TABLE VI
QUALITATIVE MPPT PERFORMANCE COMPARISON SUMMARY

	[7]	[12]	[13]	[19]	Proposed method
Classification Type	Customized Algorithm	Sensorless and Memoryless P&O Variation	Memory enhanced P&O	Artificial neural network enhanced P&O	Memory enhanced P&O
Adapts to machine aging	No	Yes	Yes	Yes	Yes
Complexity	Low	Low	Medium	High	Medium
MPP search time	Fast	Slow	Moderate	Slow	Fast
Robust to atmospheric change	Yes	No	No	Yes	Yes
Accuracy	High	Moderate	Moderate	High	High
Memory/ Computation Requirement	N/A	Low	Moderate	High	Moderate

IV. CONCLUSION

In this paper, an intelligent parameter-independent power management controller has been presented for standalone off-grid small wind energy systems. With the state observer presiding over the SA MPPT and the PLS in the proposed controller, the convergence times to the desired operating points is reduced and the logical errors are minimized by identifying the changes in wind conditions. Being applicable for both grid-connected and standalone wind systems, the SA MPPT increases a wind system's MPP search efficiency and enables the wind system to actively adapt to its changing behavior and wind conditions. The PLS algorithm was designed to complement the SA MPPT for standalone wind systems that have limited energy storage and use energy dissipation mechanisms to disperse surplus energy. Rather than focusing on capturing maximum power, the PLS focuses on reducing the size and heat requirements of the energy dissipation mechanism by minimizing surplus power generation as desired. The operating principles of the proposed PLS and MPPT control techniques have been discussed in this paper. Simulation results on a 3-kW system and experimental results on a proof-of-concept prototype with a wind turbine emulator have been provided to highlight the merits of this paper.

REFERENCES

[1] Global Wind Energy Council, "Global wind report—Annual market update 2012," 2013.
[2] Global Wind Energy Council, "Global wind 2011 report," 2012.
[3] Canadian Wind Energy Association. Canadian wind energy association (2015). [Online]. Available: www.canwea.ca

[4] Q. Wang and L. Chang, "An intelligent maximum power extraction algorithm for inverter-based variable speed wind turbine systems," *IEEE Trans. Power Electron.*, vol. 19, no. 5, pp. 1242–1249, Sep. 2004.
[5] E. Koutroulis and K. Kalaitzakis, "Design of a maximum power tracking system for wind energy conversion applications," *IEEE Trans. Ind. Electron.*, vol. 53, no. 2, pp. 486–494, Apr. 2006,
[6] J. Hui and A. Bakhshai, "A new adaptive control algorithm for maximum power point tracking for wind energy conversion systems," in *Proc. IEEE Power Electron. Spec. Conf.*, 2008, pp. 4003–4007.
[7] K. Kim, T. Van, D. Lee, S. Song, and E. Kim, "Maximum output power tracking control in variable-speed wind turbine systems considering rotor inertial power," *IEEE Trans. Ind. Electron.*, vol. 60, no. 8, pp. 3207–3217, Aug. 2013.
[8] S. Morimoto, H. Nakayama, M. Sanada, and Y. Takeda, "Sensorless output maximization control for variable-speed wind generation system using IPMSG," *IEEE Trans. Ind. Appl.*, vol. 41, no. 1, pp. 60–67, Feb. 2005.
[9] A. Mesemanolis, C. Mademlis, and I. Kioskeridis, "Optimal efficiency control strategy in wind energy conversion system with induction generator" *IEEE J. Emerg. Sel. Topics Power Electron.*, vol. 1, no. 4, pp. 238–246, Dec. 2013.
[10] R. Datta and V. Ranganathan, "A method of tracking the peak power points for a variable speed wind energy conversion system," *IEEE Trans. Energy Convers.*, vol. 18, no. 1, pp. 163–168, Mar. 2003.
[11] K. Tan and S. Islam, "Optimum control strategies in energy conversion of PMSG wind turbine system without mechanical sensors," *IEEE Trans. Energy Convers.*, vol. 19, no. 2, pp. 392–399, Jun. 2004.
[12] Y. Zhao, C. Wei, Z. Zhang, and W. Qiao "A review on position/speed sensorless control for permanent-magnet synchronous machine-based wind energy conversion systems" *IEEE J. Emerg. Sel. Topics Power Electron.*, vol. 1, no. 4, pp. 203–216, Dec. 2013.
[13] Y. Xia, K. Ahmed, and B. Williams, "A new maximum power point tracking technique for permanent magnet synchronous generator based wind energy conversion system," *IEEE Trans. Power Electron.*, vol. 26, no. 12, pp. 3609–3620, Dec. 2011.
[14] A. Knight and G. Peters, "Simple wind energy controller for an expanded operating range," *IEEE Trans. Energy Convers.*, vol. 20, no. 2, pp. 459–466, Jun. 2005.
[15] Z. Dalala, Z. Zahid, W. Yu, Y. Cho, and J. Lai, "Design and analysis of an MPPT technique for small-scale wind energy conversion systems," *IEEE Trans. Energy Convers.*, vol. 28, no. 3, pp. 756–767, Aug. 2013.
[16] V. Yaramasu and W. Bin, "Predictive control of a three-level boost converter and an NPC inverter for high-power PMSG-based medium voltage wind energy conversion systems," *IEEE Trans. Power Electron.*, vol. 29, no. 10, pp. 5308–5322, Oct. 2014.
[17] J. Chen, J. Chen, and C. Gong, "New overall power control strategy for variable-speed fixed-pitch wind turbines within the whole wind velocity range," *IEEE Trans. Ind. Electron.*, vol. 60, no. 7, pp. 2652–2660, Jul. 2013.
[18] Z. M. Dalala, Z. U. Zahid, and J.-S. Lai, "New overall control strategy for small-scale WECS in MPPT and stall regions with mode transfer control," *IEEE Trans. Energy Convers.*, vol. 28, no. 4, pp. 1082–1092, Dec. 2013.
[19] C. Wei, Z. Zhang, W. Qiao, and L. Qu, "Intelligent maximum power extraction control for wind energy conversion systems based on online Q-learning with function approximation," in *Proc. IEEE Energy Convers. Congr. Expo.*, 2014, pp. 4911–4916.
[20] M. Cirrincione, M. Pucci, and G. Vitale, "Neural MPPT of variable-pitch wind generators with induction machines in a wide wind speed range," *IEEE Trans. Ind. Appl.*, vol. 49, no. 2, pp. 942–953, Apr. 2013.
[21] N. Mendis, K. M. Muttaqi, S. Perera, "Management of Low- and high-frequency power components in demand-generation fluctuations of a DFIG-based wind-dominated RAPS system using hybrid energy storage," *IEEE Trans. Ind. Appl.*, vol. 50, no. 3, pp. 2258–2268, Jun. 2014.
[22] J. Hui and P. K. Jain, "Power management and control of a wind energy conversion system (WECS) with a fuzzy logic based maximum power point tracking (MPPT)," in *Proc. IEEE 38th Annu. Conf. Ind. Electron. Soc.*, 2012, pp. 5966–5971
[23] N. Mendis, K. M. Muttaqi, S. Sayeef, and S. Perera, "Standalone operation of wind turbine-based variable speed generators with maximum power extraction capabilitym," *IEEE Trans. Energy Convers.*, vol. 27, no. 4, pp. 822–834, Dec. 2012.
[24] S. Sharma and B. Singh, "Asynchronous generator with battery storage for standalone wind energy conversion system," *IEEE Trans. Ind. Appl.*, vol. 50, no. 4, , pp. 2760–2767, Jul. 2014.
[25] A. M. O. Haruni, M. Negnevitsky, M. E. Haque, and A. Gargoom, "A novel operation and control strategy for a standalone hybrid renewable power system," *IEEE Trans. Sustainable Energy*, vol. 4, no. 2, pp. 402–413, Apr. 2013.
[26] N. Mendis, K. M. Muttaqi, and S. Perera, "Management of battery-supercapacitor hybrid energy storage and synchronous condenser for isolated operation of PMSG based variable-speed wind turbine generating systems," *IEEE Trans. Smart Grid*, vol. 5, no. 2, pp. 944–953, Mar. 2014.
[27] Z. Lubosny, *Wind Turbine Operation in Electric Power Systems*. New York, NY, USA: Springer-Verlag, 2003

Joanne C. Y. Hui (S'08–M'14) received the B.Sc. (Hons.), M.Sc. (Eng.), and Ph.D. degrees from Queen's University, Kingston, ON, Canada, in 2006, 2008, and 2014, respectively.

She was a Design Engineer with SPARQ Systems, Inc., Kingston, from 2011 to 2013. She is currently a Postdoctoral Research Fellow with the Queen's Center for Energy and Power Electronics, Queen's University. She has authored more than 20 IEEE conferences and journal papers. Her current research interests include optimal power extraction and energy management algorithms for renewable energy applications and smart microgrids.

Dr. Hui received the Ontario Graduate Scholarship from 2010 to 2011 and the Ontario Graduate Scholarship in Science and Technology from 2008 to 2009 and 2009 to 2010. She was the Topic Chair in the 2015 IEEE Energy Conversion Congress and Exposition.

Alireza Bakhshai (M'04–SM'09) received the B.Sc. and M.Sc. degrees from the Isfahan University of Technology, Isfahan, Iran, in 1984 and 1986, respectively, and the Ph.D. degree from Concordia University, Montreal, QC, Canada, in 1997.

He was a Faculty Member with the Department of Electrical and Computer Engineering, Isfahan University of Technology, from 1986 to 1993 and 1998 to 2004. From 1997 to 1998, he was a Postdoctoral Fellow with Concordia University. He is currently with the Department of Electrical and Computer Engineering, Queen's University, Kingston, ON, Canada. His current research interests include high-power electronics and applications in distributed generation and wind energy, control systems, and flexible ac transmission services.

Praveen K. Jain (S'86–M'88–SM'91–F'02) received the B.E. (Hons.) degree from the University of Allahabad, Allahabad, India, in 1980, and the M.A.Sc. and Ph.D. degrees from the University of Toronto, Toronto, ON, Canada, in 1984 and 1987, respectively, all in electrical engineering.

He made pioneering contributions in introducing resonant power conversion technology in telecommunications during his work with Nortel, Montreal, QC, Canada, in the 1990s. He played a key role in the design and development of high-frequency power conversion equipment for the International Space Station at Canadian Astronautics in the late 1980s. Over the last 30 years, he has made sustained contributions to the theory and practice of power electronics through his considerable work with the industry, including Astec, Freescale, General Electric, Intel, and Nortel. He is currently a Professor of electrical and computer engineering with Queen's University, Kingston, ON, Canada, the Tier 1 Canada Research Chair in Power Electronics, and the Director of the Queen's Centre for Energy and Power Electronics Research. He is the Founder of two successful start-up companies, such as CHiL Semiconductor, Tewksbury, MA, USA, where he is involved in digital power controller (acquired by International Rectifier), and SPARQ Systems, Kingston, where he is involved in photovoltaic microinverters. He has supervised and guided more than 85 graduate students, postdoctoral fellows, and power electronics engineers, who are well placed in the industry and academia. He has authored more than 450 papers and holds 50 patents.

Dr. Jain received the Queen's Prize for Excellence in Research, the IEEE William Newell Power Electronics Award, and the Engineering Medal of the Professional Engineers of Ontario, and was the IEEE IAS Distinguished Lecturer, and a Fellow of the Royal Society of Canada, the Engineering Institute of Canada, and the Canadian Academy of Engineering.